



HAL
open science

Light–Matter Complex Interactions in Stereolithographies

Thomas Doualle, Laurent Gallais, Jean-Claude André

► **To cite this version:**

Thomas Doualle, Laurent Gallais, Jean-Claude André. Light–Matter Complex Interactions in Stereolithographies. Applied Sciences, 2023, 13 (11), pp.6844. 10.3390/app13116844 . hal-04415642

HAL Id: hal-04415642

<https://cnrs.hal.science/hal-04415642>

Submitted on 14 Feb 2024

HAL is a multi-disciplinary open access archive for the deposit and dissemination of scientific research documents, whether they are published or not. The documents may come from teaching and research institutions in France or abroad, or from public or private research centers.

L'archive ouverte pluridisciplinaire **HAL**, est destinée au dépôt et à la diffusion de documents scientifiques de niveau recherche, publiés ou non, émanant des établissements d'enseignement et de recherche français ou étrangers, des laboratoires publics ou privés.

Light–Matter Complex Interactions in Stereolithographies

Thomas Doualle ¹, Laurent Gallais ¹ and Jean-Claude André ^{2,*}

¹ Aix Marseille Univ, CNRS, Centrale Marseille, Institut Fresnel, Avenue Escadrille Normandie-Niemen, 13397 Marseille, France; thomas.doualle@cea.fr (T.D.); laurent.gallais@fresnel.fr (L.G.)

² Université de Lorraine, CNRS, LRGP, 1, rue Grandville, 54000 Nancy, France

* Correspondence: jean-claude.andre@cnrs.fr

Featured Application: 3D printing.

Abstract: Since its inception in 1984, 3D printing has revolutionized manufacturing by leveraging the additivity principle and simple material–energy coupling. Stereolithography, as the pioneering technology, introduced the concept of photopolymerization with a single photon. This groundbreaking approach not only established the essential criteria for additive processes employing diverse localized energies and materials, including solid, pasty, powdery, organic, and mineral substances, but also underscored the significance of light–matter interactions in the spatial and temporal domains, impacting various critical aspects of stereolithography’s performance. This review article primarily focuses on exploring the intricate relationship between light and matter in stereolithography, aiming to elucidate operational control strategies for fabrication processes, encompassing voxel size manipulation. Furthermore, advancements in light excitation modes, transitioning from one-photon to two-photon mechanisms, have unlocked new material and creative possibilities. Notable advantages include the elimination of layering (true 3D printing) and the ability to fabricate objects using silica glass. Although these volumetric 3D printing methods deviate from conventional additive manufacturing concepts and possess narrower application scopes, they offer reduced manufacturing and design timeframes along with enhanced spatial resolution in select cases. These complex light–matter interactions form the cornerstone of this comprehensive review, shedding light on operational control strategies and considerations in stereolithography. By comprehensively analyzing the impact of light–matter interactions, including the novel two-photon excitation, this review highlights the transformative potential of stereolithography for rapid and precise fabrication. While these techniques may occupy a smaller niche within the broader spectrum of 3D printing technologies, they serve as valuable additions to the array of 3D devices available in the market.

Keywords: 3D printing; two-photon absorption; printability; chemical kinetics; materials



Citation: Doualle, T.; Gallais, L.; André, J.-C. Light–Matter Complex Interactions in Stereolithographies. *Appl. Sci.* **2023**, *13*, 6844. <https://doi.org/10.3390/app13116844>

Academic Editor: Zhonghua Sun

Received: 8 April 2023

Revised: 27 May 2023

Accepted: 28 May 2023

Published: 5 June 2023



Copyright: © 2023 by the authors. Licensee MDPI, Basel, Switzerland. This article is an open access article distributed under the terms and conditions of the Creative Commons Attribution (CC BY) license (<https://creativecommons.org/licenses/by/4.0/>).

1. Introduction

The basic idea of additive manufacturing or 3D printing is presented in Figure 1. It involves an energetic stimulation to create an elementary volume called a “voxel” (different in terms of the nature of the initial material), which, when moved in space, leads to a series of voxels that only becomes a 3D object if there is sufficient cohesion between the voxels (notion of printability).

Because we have known for a long time how to “play” with the energy of light, it was first possible to imagine a transformation of matter by the energy carried by light: polymerization by electronic excitation of a resin, thermally induced polymerization, etc. Under these conditions, we go from a fluid (the resin) to a solid voxel. In the first patent, in 1984 [1], the authors had not yet studied the evolution of the chemically-induced resolution on the final result. Thus, the global resolution is an association between two interdependent phenomena, one related to the light power present at a point in space, the other to the polymerization chemistry (and especially to its exothermicity).

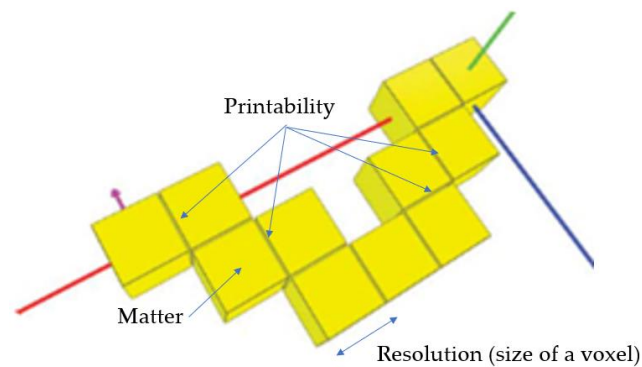


Figure 1. The fundamentals of additive manufacturing.

If today there are other ways of energy stimulation (seven major families of additive manufacturing processes) [2], the processes using light retain their interest in many areas such as micro-fabrication, production of prototype parts, bio-printing, indirect realization of parts in their material of use (ceramics, glasses, etc.), etc. Obviously, the performances that are achieved depend on the methodologies that affect the spatial resolution and printability aspects presented above.

After having reviewed the interest in photopolymerizable resins whose transformation results from chain reactions, the focus is then put on the aspects of optical resolution which depend on the modes of electronic excitation of photochemical initiators or on the heat transfers for thermal initiators and depend on the resins and their possible charges. The “printability” aspect is also discussed, as it conditions the realization of real objects. Light can play different roles in terms of initiating chain polymerization reactions (which in principle corresponds to an amplification process). This document considers first of all, the initiation process, the material aspect, and the reaction schemes. A remark is made in this part concerning a thermal initiation which allows, in particular, conditions for the realization of 3D parts. Apart from the material aspect, the emphasis is put on what represents the volume of interaction between the transformable matter and the process of light excitation with one photon, or two photons absorbed simultaneously or sequentially. These volumes are connected with the voxel forms and sizes. These modes lead to specific performances and to the control of associated processes. Finally, in these different presentations, the authors try not to forget that these are manufacturing technologies with technical, financial, and optimization constraints.

2. Resins and Additive Manufacturing

With acrylic type resins, it is possible to carry out chain radical polymerizations. However, these are protected by inhibitors, which, in continuous excitation with a photon lead to complex polymerization kinetics that must be taken into account in the realization of a voxel. This mechanistic aspect is the starting point of this part dedicated to the resins used in stereolithography. Before dealing with the consequences of the light–matter relationships, a singular point is underlined, that of the exothermicity of the polymerization reactions which can be taken advantage of, but with the risk of a loss in spatial resolution.

In principle, it is possible to provide energy locally to carry out a chemical transformation (here, a radical chain polymerization). The chemical kinetics of radical polymerization reactions corresponds to a nonlinear process, qualitatively presented in Figure 2 [2,3]. Photochemical radical polymerization has a threshold behavior. Under these conditions, if one knows how to have a different light intensity from one point in space to another, or a sufficient exposure time, or finally an inhibitor concentration from one element in space to another, etc., the polymerization can be spatially controlled. The weakly irradiated regions do not contribute to the polymerization as long as one is zone I (presented in Figure 2; it corresponds to the total non-consumption of the inhibitors of radical polymerization, in particular of oxygen).

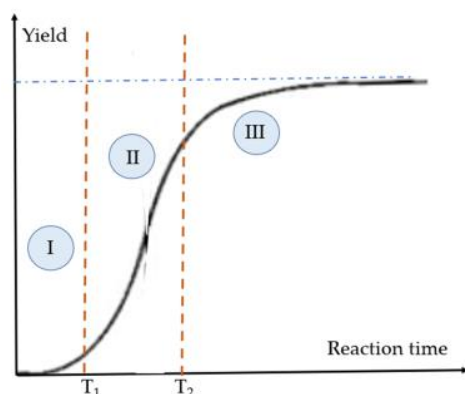


Figure 2. Typical polymerization kinetic curve under continuous irradiation. Phase I: very slow kinetics related to the consumption of the inhibitor(s); phase II: radical polymerization before reaching the gel point; phase III: cross-linking of the multifunctional monomer links.

Figure 3 [2,4] schematically represents a reaction (with its very simplified mechanism) of radical chain polymerization that allows, from a free radical created by any photonic or thermal process, the transformation of a large number of molecules (monomers and/or oligomers).

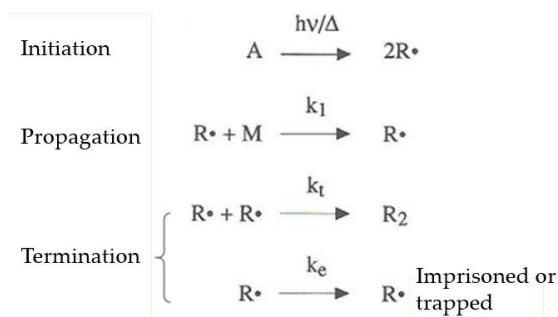


Figure 3. Radical mechanism of chain polymerization (A corresponds to the initiator producing free radicals R. reacting with the monomer M under light ($h\nu$) or thermal (Δ) initiation).

To store the resins, they must be stabilized with conventional free radical polymerization inhibitors. Dissolved oxygen also has the same role. To those elements of the reaction mechanism presented in Figure 3, it is necessary to add a complementary process of consumption of the inhibitors Q (chemical rate constant k_q):



In practice, the photochemical initiator is a conventional commercial ketone-type initiator and the resins are typically from the multifunctional acrylic family.

2.1. Materials

Several situations have been observed since 1984 [1]:

- The photopolymer must not dissolve in the resin that gave birth to it, which requires multifunctional monomers (see Figure 4);
- The polymer is generally denser than the initial monomer, which leads to shrinkage (as in foundry); and if the object was not supported, it falls (Stokes' law) to the bottom of the reactor by being deformed;
- A complex deformation linked to the manufacturing process (anisotropy of local tensions and global deformation);
- An obligation of post-treatment with the risk of an ageing likely to lead to the destruction in a few days of the realized object.

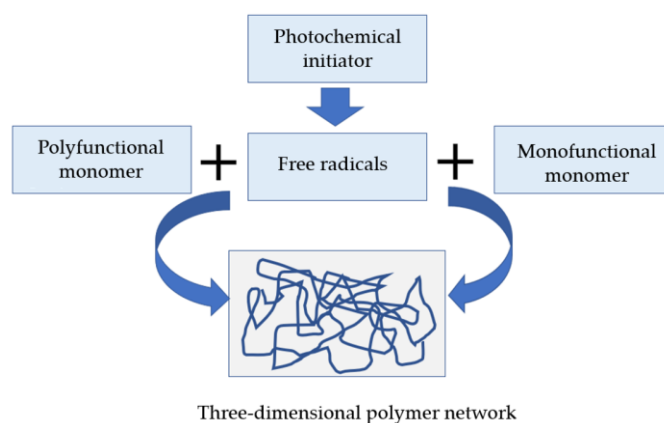


Figure 4. Radical photopolymerization of acrylic resins.

On this broad basis, the materials are commercially available and are summarized in Table 1.

Table 1. Some resins applicable in stereolithography.

Some Commercial Resins	References
Monomers, initiators: Acrylic resins and photochemical initiators (aromatic ketones). Examples: 2-hydroxyethyl methacrylate, 1,6-hexanediol diacrylate, pentaerythritol tetra-acrylate, etc.	Cf. Fluka; Sigma-Aldrich (St. Louis, MO, USA); Quick-Parts; Merck; Arkema; Norland; Yosra; Nanoscribe catalogs (2022)
Specific monomer: Ionic polymerization monomer	[5]
Commercial resins: Materialise, Acura AMX, Durable natural 3D printing resin (3D Systems), etc.	Materialise (2022); [6]; Additive 3D (2022); Evonik catalog; 3D Ceram (2022)

Table 1 should be seen as a wealth of choices of resins that can be made by the experimenter or obtained ready-made. Thus, only a few references are presented there. Industrial 3D machine manufacturers offer the opportunity to purchase their own resin that broadly meets the user's specifications [7,8]. They provide the expertise and industry knowledge necessary to accurately assess specific customer requirements and recommend/sell the most appropriate 3D printing products. The links between the process and materials processed in the same company give the company an unparalleled ability to provide a "complete value chain". This raises the difficult question of choice, which depends on the nature of the objects to be manufactured [9].

For example, Merck [10] proposes photochemical initiators such as Irgacure (2-Hydroxy-4'-(2-hydroxyethoxy)-2-methylpropiophenone) or ketone compounds of the same family, Von Raumer et al. [11] benzophenone, and Sigma-Aldrich [12] thermal initiators such as AIBN (2,2'-Azobis(2-methylpropionitrile)) and benzoyl peroxide [13].

2.2. Polymerization

In the presence of light, free radicals are produced; they consume the inhibitors and then react with the monomers to create macro-radicals which grow by reaction with "fresh" monomers with the risk of trapping free radicals in the polymer matrix. Given the concentration of monomers (quasi-pure monomer medium at the time of initiation), the polymerization takes place from close to close, on a molecular scale as shown in Figure 5. In addition, if multifunctional monomers are available, the polymer that is built up is normally insoluble in the monomer that gave rise to it [14].

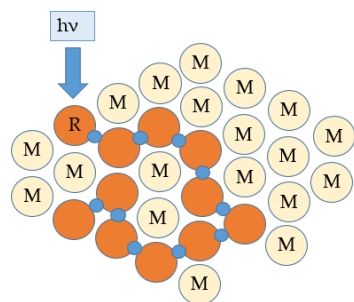


Figure 5. Spatial proximity polymerization ($h\nu$ represents the energy of the photon, where ν is the frequency of the radiation and h is Planck's constant, for a one-photon initiation). The red discs represent the elements that have reacted to form a polymer and M represents a monomer molecule.

From a chemical kinetics point of view, the transformation follows a sigmoidal law, as presented in Figure 2, with an initially slow kinetics linked to the consumption of reaction inhibitors (hydroquinone for example to allow the conservation of monomers, oxygen in solution, etc.), i.e., a “free” polymerization reaction, but increasingly hindered by the three-dimensional polymer that forms, which limits the space available for the reaction of macro-radicals with the remaining monomers and thus the reaction kinetics [15]. Experimentally, it is possible to show that then free radicals are present but are trapped in the polymeric matrix. To summarize, there are essentially three zones in such polymerization kinetics:

- a zone (I) with very slow kinetics where the free radicals formed in the initiation step consume the inhibitors (oxygen);
- the zone (II) of the polymerization itself;
- the terminal step, linked to the imprisonment of the free macro-radicals which can no longer reach the reactive bonds of the remaining monomers because of the passage from a fluid material to a highly polymerized entity in which the diffusion of the reactive species is strongly hindered (cf. Figure 5).

From an epoxy composition (cationic monomer) and a photo-initiator, polymerization under light irradiation leads to the desired liquid/solid transformation. Some compositions suitable for one-photon additive manufacturing are commercially available. These compositions include monomers, typically epoxies, and the initiator. In addition to the epoxy family of compounds, a large number of monomers are described synthetically in [16,17].

2.3. Exothermicity

Polymerization reactions are generally exothermic and there can be a local (and temporary) rise in temperature which can induce a change in the refractive index of the polymerizable liquid and then of the solid state polymer. Depending on the transparency of the resin, it is practically no longer possible to consider that the path of the light follows a straight line beyond several centimeters (loss in resolution or transformation). Under these conditions, it is necessary to build forms of object adapted to avoid the problems mentioned above or to work under spatial and/or chemical conditions where these phenomena are not preponderant or likely to be masked. This goal can be obviously achieved if one wants to create, for example, small objects, which is well suited for commercial picosecond lasers and microscopes.

There exists a critical distance for thermal polymerization. To take into account the phenomena involved, it is possible to consider a spherical structure consisting of a polymer at a temperature T_1 , bathed in a liquid medium containing the monomer and its thermal initiator at a temperature T_2 , lower than T_1 . Initiation by AIBN or benzoyl peroxide starts at a temperature between T_1 and T_2 . If the radius of the sphere is small, with a high surface to volume ratio, the heat from the sphere must dissipate before the thermal initiator has time to produce free radicals. On the other hand, for high values of this radius, the heat transfer has time to generate free radicals and provide additional heat energy that drives the polymerization from the edges of the sphere into the space accessible for the reaction.

We can therefore imagine the existence of a critical radius that corresponds to the escape of the reaction from the space that was intended for it. Moreover, from one voxel to another, the reaction medium heats up, which can lead to minor or major losses of resolution.

Then, choosing a space of spherical symmetry and an initial temperature $\theta_0 = 50\text{ }^\circ\text{C}$, Figure 6 plots the spatial variations in temperature as a function of dimensionless time τ (equal to the product of time times the thermal diffusion coefficient divided by the spot of the squared radius R of an electromagnetic wave). With a thermal initiator such as benzoyl peroxide or AIBN [18], after a dimensionless time on the order of unity, the heat, initially carried uniformly in the sphere of radius R , can be considered dissipated throughout the reactant fluid. The polymerization reaction could have started, but stops by quenching (hence no loss in spatial resolution).

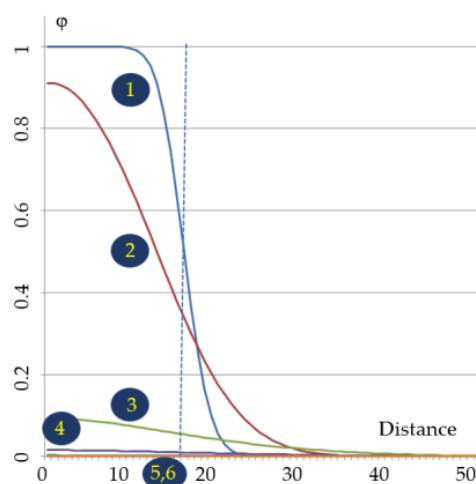


Figure 6. Temperature variations during the dimensionless polymerization time for $\theta_0 = 50\text{ }^\circ\text{C}$. Relative temperature (φ) beyond θ_0 is represented on the ordinate; on the abscissa, 100 units represent $5 \times R$ (i.e., in our conditions, 0.5 mm). 1: $\tau = 0.01$; 2: $\tau = 0.1$; 3: $\tau = 1$; 4: $\tau = 2$; 5: $\tau = 3$; 6: $\tau = 5$.

These results can be obtained from the chemical kinetics data of references [16,19–22].

At the same time, it is possible to represent, all other things being equal, the conversion rate, as a function of time and space, of the monomer (Figure 7). This figure illustrates that a limit is reached as soon as the dimensionless time is of the order of one unit (see above).

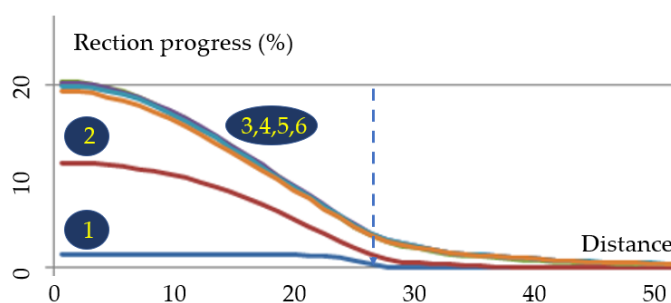


Figure 7. Variations in monomer concentration for different dimensionless times related to polymerization for $\theta_0 = 50\text{ }^\circ\text{C}$ and $\theta_1 = 150\text{ }^\circ\text{C}$ (by heating the irradiated area). Polymerization advancement (%) is shown on the ordinate; on the abscissa, 100 units represent $5 \times R$ (i.e., in our conditions, 0.5 mm). 1: $\tau = 0.01$; 2: $\tau = 0.1$; 3: $\tau = 1$; 4: $\tau = 2$; 5: $\tau = 3$; 6: $\tau = 5$.

It is with a thermal effect of this type that it is possible to produce 3D objects using infrared (CO_2) lasers [23,24] from a layered process allowing heat transfer outside the polymerization zones. However, by seeking to polymerize voxels larger than about 1 cm, the heat-producing polymerization reaction results in polymerization of the entire resin content of the reactor, as shown in Figure 8.



Figure 8. Thermally cured part in a conductive sleeve. All the material accessible to the exothermic reaction is transformed into the polymer (see photograph on the right).

What these simplified models and experiments with thermal initiators show, is that the theoretical space corresponding to the light–matter interaction can be deeply perturbed by exogenous elements: the presence of an inhibitor, consumption of the quencher, thermal effects, etc. These elements must be taken into account to define robust stereolithography processes.

2.4. Resolution

Provided that a reaction is not degenerate (see Figure 8), i.e., limited to initiation, with chain lengths of about 100 and monomer size of 5 nm, it is under the best possible conditions conceivable to occupy an approximate volume of $100 \times 125 \text{ nm}^3$, corresponding to a cubic voxel size of the order of 20–25 nm on a side. On this basis, it is not the chemistry that limits the spatial resolution.

2.5. Initiation Time

Assuming a time-independent rate of chain-bearing radical production (R_0), the Q inhibitors are in a situation where their concentration decreases before cancelling out, corresponding to:

$$R_0 = 2kt \cdot (R \cdot)^2, \quad (2)$$

After some mathematical manipulations, the mechanism proposed in Figure 3 and its kinetic consequences lead to a characteristic time T_1 , defined by:

$$T_1 = ((2kt/R_0)^{1/2})/kq \quad (3)$$

This result shows that T_1 is lower the higher R_0 is. This is the same for kq . We will come back later to the importance of the excitation modes of the initiators and their spatial distribution on T_1 .

2.6. Composites

The additive manufacturing discussed here results from a transformation of a liquid into a solid under the action of electromagnetic radiation. The fillers that can be included in the monomer must be small [25] for various reasons, at least one of which is related to Stokes' law, associated with the size of particles subject to the gravitational effect. With large particles, with passive and long-term storage of reagents, all charges can be at the bottom of the fabrication device. We also suppress shadow effects that can be detrimental to the mechanical quality of 3D objects thus realized. If the effect associated with Stokes' law is present in the layers (initial process of stereolithography), the 3D object will have strongly anisotropic mechanical properties. Indeed, additive manufacturing (AM) refers to “a process in which materials are assembled, usually layer by layer, to make an object that conforms to the 3D data that model it” [2,17].

A structural composite material is generally composed of a reinforcement and a matrix. The reinforcement, most often in fibrous or filamentary form, provides the essential mechanical properties [26]. However, in another context, when it comes to “green” parts, for example in ceramic production, it is not the mechanical strength that is strictly sought

but the possibility of a part with little deformation that, by various operations (de-binding, sintering), will lead to the final usable part. The matrix plays the role of binder to protect the reinforcement from the environment, to maintain it in its initial position, and to ensure the transmission of forces. Composite materials can be classified according to the nature of their matrix: organic matrix, ceramic matrix, or metal matrix composite material. In fact, as indicated by [27], all powdered materials can be considered, even lunar dust.

This context, as defined above, is based on the principle of printability (deep association of voxels as shown in Figure 1 by adherence), and thus raises the question of the quantity of filler that will allow the desired performance to be obtained in the composite. What happens when the fillers are no longer fully associated with their carrier polymer? With mono-dispersed spheres (simplifying assumption), the interparticle porosity ε represents the fraction of the volumes between spheres relative to the volume of the considered set. If ρ_{app} and ρ_{sol} represent the bulk and bulk solid densities, then:

$$\varepsilon = 1 - \rho_{app} / \rho_{sol} \quad (4)$$

This depends on the organization of the spheres and is of the order of 45%. For mono-dispersed hard spheres, the space can be filled with a variable number of spheres, as shown in Figure 9. In fact, between materials and their shapes, there are, independently of the stimulation modes, an infinite number of possibilities. Hence, the interest in using a more poly-dispersed population to improve on this aspect which, obviously, will result in a consequent volume shrinkage [2]: the small particles can fill the spaces between the larger ones, which decreases ε . Beyond a certain threshold, this advantage disappears, to recover, for an infinite dilution of the large ones, the initial value of ε [28]. It is possible to find size distributions so that the space is maximally occupied. However, it is not practically possible to achieve, with divided solids, the compactness of a massive solid [29,30].

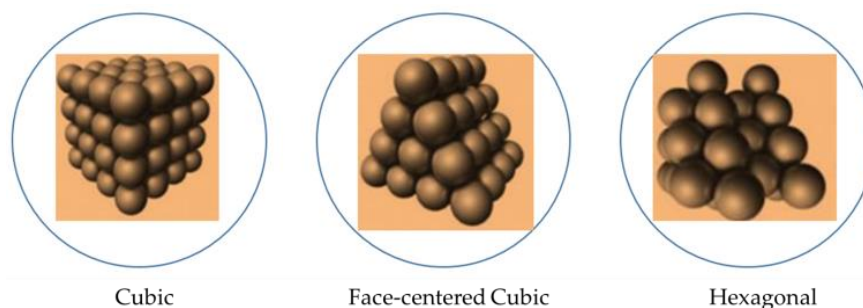


Figure 9. Density linked to regular stacks of spheres (according to <http://villemmin.gerard.free.fr/Wwwgymm/Geometri/SpheEmpi.htm>, accessed on 22 March 2023)—with the possibility of linking the spheres representing the charges by capillarity and polymerization.

Granular materials pile up on top of each other and self-lock to the point where they sometimes experience a vault effect that stops all flow [31]. To break this vault, a vibration can sometimes be enough. Compacted to the maximum, the granular materials retain a void between them representing about 25% of the total volume. Figure 10 represents the ideal case of “Apollonian” stacking (Apollonius of Perge having lived in the 2nd century BC), which is far from reality which must take into account the morphology of the powders. For a situation of this type, the behavior of the stacking is practically that of a massive solid, which can pose issues of realization of the layers of particles necessary to the 3D process. The viscosity of the resin–filler couple is an increasing function of the quantity of the filler. Independently of this physical aspect, the surface condition of the particles can have a determining role on the stacking. This can depend on the storage with possible surface oxidations, the effect of humidity, etc. [32]. This is important because it can have an effect on the quality of objects made from certain powdered materials.

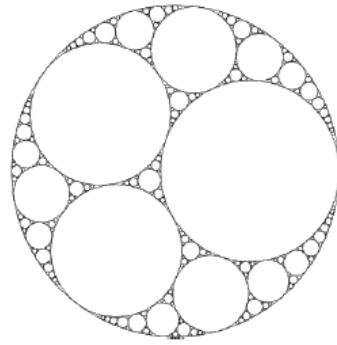


Figure 10. Apollonian stacking.

However, in the case of Figure 10, the assembly is basically that of a solid. The classical one-photon stereolithography process is a layer-by-layer process. It is therefore necessary to find compromises between the density of the charge ε and the time required to set up the layers.

It is thus understood that there is no simple way to easily suppress the trapping of bubbles in the sintered or molten material since the total compactness cannot be theoretically reached. On the other hand, these phenomena do not occur, or only to a limited extent, with a charge-liquid resin mixture. In any case, the shrinkage aspects are part of the issues to be addressed in terms of programming the manufacture of the object (reverse engineering), but in the case treated, if the resin has a shrinkage, the passive fillers limit the effect.

2.7. Conclusions

If resins, in particular of the acrylic family, are good candidates for stereolithography, their transformation from fluid to solid (independently of the rheological aspects of the layer process) follows complex reaction kinetics, depending on the number of photons absorbed locally. Apart from problems related to the exothermic conditions of the polymerization reactions, this chemical process has no major effect on the 3D resolution, which has allowed the realization of 3D parts in μ -stereolithography. In addition, a focus is placed on the charged resins that are increasingly used in the realization of “green” 3D parts for the creation of ceramic objects.

3. Printability

The fact of placing voxels against each other undoubtedly makes it possible to reach a shape, but the adhesion between the various elementary volumes is an important element so that the 3D part is regarded as acceptable: this objective can be reached by gluing (polymerization), heating, assembly, etc. These successful operations qualify the performance of the part.

3.1. General Considerations

Apart from systems cut from a block of material or made by 3D printing with a single material (such as in this paper), the manufacture of a 3D structure generally involves the assembly of parts that are glued together, this bonding is normally included in the process. This is what is described in this article, with a bonding made with the same monomeric material, as has been abundantly explained, the voxel being created has a size greater than the volume of material to be transformed. It can be the same for multi-material printing with voxels having a variable adhesion between them. Thus, a structure made up of different elements, in particular in the nature of the materials used to realize them, is built by the cohesive assembly of these various voxels. It is natural to think that the more complex the structure is, the higher the number of parts to be assembled and necessary to build the structure. It is therefore necessary to consider, at least partially, the printability of materials in the process of additive manufacturing being considered.

As a reminder, beyond making it possible to achieve the shape of a structure, the assembly ensures the transmission of loads from one voxel to another, and therefore the assembly technique becomes a major factor (hence the concept of printability). There are many assembly methods in the industry, but generically the three main structural assembly techniques are welding, gluing, and bolting/riveting. Apart from gluing, these are not very well adapted to the cohesion of voxels, especially with sub-millimeter resolutions, which requires seeking a compatibility between voxels of different origins so that the associated printability allows, in one step, the 3D object to adapt to the solicitations applied to the multi-material 3D structures in relation to the particular functions that they have to fulfill. Another method is the use of a complementary interface that connects the voxels by gluing; then, the mechanical strength of the 3D assembly will obviously depend on the nature of the glue and the surfaces of the glued materials, but also on the mode of mechanical solicitation applied.

Without going too far into the concept of printability, it is useful to return to the general principles of bonding [33], which involve different elements:

- Mechanical: The adhesive will lodge in the pores, the asperities of the voxels. The roughness of the voxel and the notion of wetting are involved;
- Diffusion: Adhesion occurs by the progressive disappearance of the interface. It is the inter-diffusion of the macromolecules that achieves the adhesion. This diffusion obeys the classical parameters: molecular weight, polarity, crystallinity, degree of cross-linking, glass transition temperature.

Bretton and Villoutreix [34] present the properties of the main structural and non-structural adhesives available to date, as well as the problems raised by the use of bonding in industrial manufacturing.

3.2. Acrylic Resins

In 1984, in the first patent concerning stereolithography [1], it was possible to make it very simple by defining layers of photopolymerizable resins. Under these conditions, the surface in contact with the ambient air remained fluid for a few μm and it was only after the realization of the upper layer that the oxygen was trapped, not renewed, and consumed. This chemical disadvantage thus became an advantage in the process by allowing the bonding of the layers to each other. Since then, other additive manufacturing technologies have been developed [2]. For light absorption inside the reaction volume, we find the presence of inhibitors that, once irradiated are consumed, and allow polymerization. The object is thus constituted without discontinuity of the same polymer. Moreover, it had been shown by Schaeffer et al. [35] that during the construction of the object, the next voxel is “stuck” to the previous one while its polymerization occurs in the zone between T_1 and T_2 , that is to say, with a still soft and reactive material (see also [14]).

3.3. Conclusions

In additive manufacturing processes, an energy input, normally localized in space and time, is necessary for a 3D object to be built. The notion of printability goes a little further, since it considers the object placed in its real conditions of use.

4. Production of Free Radicals by Light

By absorbing a photon of suitable energy (of the order of magnitude of the energy of a chemical bond) in one or two steps, light can cause the production of free radicals. By going back to the fundamentals of light absorption processes, this part reminds us what the associated laws are, in particular by introducing the concept of optical thickness, μ , for transparent and charged media. The effect of the time of continuous one-photon or pulsed two-photon irradiation is also treated in this part leading to mastered voxel size relationships with the principal parameters (i.e., number of absorbed photons, μ , chemical kinetics parameters). Examples are also presented.

4.1. General Considerations

Since the works of Göppert-Mayer in 1931 [36], then those of the photo-physicists and photo-chemists, on the processes of absorption of light, in particular by organic molecules, one knows the light absorption processes with one or more photons corresponding to the promotion of an electron of an occupied orbital to another free one, leading to the promotion of a molecule into an unstable electronic excited state. The idea of the Battelle Institute in the years 1970–1985 [37,37,38] was already to fabricate three-dimensional objects in fluids, transparent to the wavelengths emitted by coherent sources, by multi-photon absorption. The principle retained at that time was to “play” on a bi- or even multi-photonic absorption such as the one presented in Figure 11.

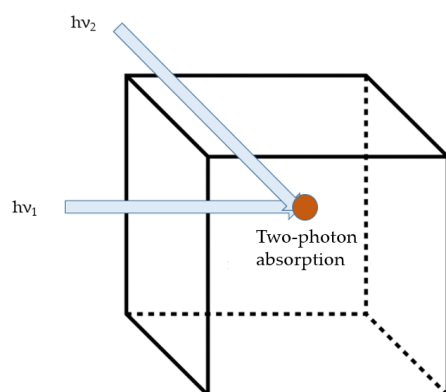


Figure 11. Principle of simultaneous or sequential two-photon absorption.

In this figure, the incident photons are represented by their energy, $h\nu$, where h is Planck’s constant and ν the frequency of the radiation. At that time, it was sequential absorption, defined as follows: a chromophore absorbs a photon of wavelength λ_1 (corresponding to the frequency ν_1 , with $\lambda = c/\nu$, where c is the speed of light in vacuum) and then has a certain lifetime (from a few picoseconds to an hour). A second photon, emitted at λ_2 , allows it to pass on a higher electronic excited state which will lead to the fragmentation of the molecule (or by energy transfer to an acceptor). Thus, relative to what has been described in stereolithography regarding the one-photon initiation of a free radical or ionic polymerization reaction, the formation of the species that will initiate the polymerization then occurs in a two-photon process in a sequential or simultaneous manner (see Figure 11). In this same figure, the principle of simultaneous absorption is represented (on the right of the figure). By moving the light beams in a transparent medium (which is generally not so simple to achieve for thicknesses of a few centimeters or tens of centimeters), one can in principle imagine operating a local transformation of the medium. This can be achieved by populating an electronic excited state precursor of the species involved in the initiation step, either by sequential absorption, requiring the transition through an intermediate electronic excited state [39], or by the formation of an unstable chemical intermediate, or simultaneously (cf. Figure 12).

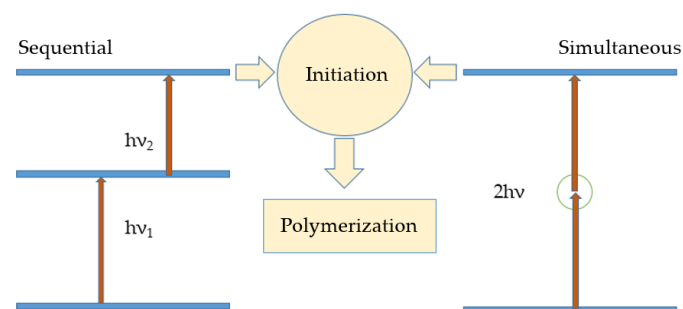


Figure 12. Sequential (left) and simultaneous (right) two-photon absorption.

We recall that if F is the luminous flux at a given wavelength, it is absorbed according to a law of the form:

$$dF/dx = -\alpha \cdot F - \beta F^2 - \gamma F^3 - \dots \quad (5)$$

The term α is classically expressed in $\text{mole}^{-1} \cdot \text{L} \cdot \text{cm}^{-1}$ (α varies depending on the electronic transitions involved, from a few units to $10^5 \text{ mole}^{-1} \cdot \text{L} \cdot \text{cm}^{-1}$) by photo-chemists and spectroscopists, β is the effective capture cross-section related to the concentration for a simultaneous two-photon absorption. This effective capture cross-section is usually expressed as GM, named after Maria Goeppert-Mayer. We recall that a GM corresponds to $1 \times 10^{-50} \text{ cm}^4 \cdot \text{s} \cdot \text{molecules}^{-1} \cdot \text{photon}^{-1}$ (as examples, the effective section of capture is 300 GM for Rhodamine B, 100 for Rhodamine, and 28 for Fluorescein). For two-photon photochemical initiators, Schafer et al. [35] report values on the order of 10–20 GM (see also [40]). Quantum rules are used to estimate this parameter [36,41–44]. One of the first advantages of this excitation mode, initially applied to microscopy of biological materials, is the quality of the spatial resolution, as shown in Dufour et al. [45]. A second, which comes out of this work, is related to the fact that the biological media studied are relatively transparent in this spectral range located between the red and the infrared.

To return to these “old” times, if the access to picosecond, or better femtosecond, lasers was envisaged, the cost of these sources was prohibitive, whereas the photochemistry of the two-photon processes had already begun to be studied, which could explain the origin of the patents of Battelle. Several possibilities could be evoked: absorption of a photon to populate an electronic singlet state, transition to a triplet state (of potentially longer lifetime than the singlet), absorption of a second photon to populate from this state another reactive triplet state (e.g., the case of acridine in [46,47]), formation of a triplet state that transfers its energy to another triplet that itself absorbs a photon to create a reactive state (acridine-rhodamine 123 couple, for example [2]). The interest of this system is that, on the one hand, if the linear transformation results in a non-radiative return without any noticeable chemical transformation, this is because the system may be reversible at low light intensities, on the other hand, the triplet–triplet absorption allows for chemical transformation of the medium with obvious possibilities in terms of spatial resolution. The reader interested in this area may benefit from consulting several other works (cf. [48]) that present values of high molecular extinction coefficients for triplet–triplet transitions, with additions from [49]; for other substances, it may be possible to consult the following references [50–55]; for diacetyl (with a high room temperature triplet lifetime of the order of one millisecond), see [56]. Whether it is a single-photon or multi-photon process, the initiation is a nonlinear process, but following very different absorption laws [14].

4.2. One-Photon Process

4.2.1. Absorption by an Unfilled Resin

With low intensity light fluxes, only the first-order term needs to be considered. This is a one-step process where an electron from a ground state orbital is promoted to an electronically excited state. The molecule in this state is assumed to produce chain-bearing free radicals. Figure 13 from [57] shows a spectrum of a benzophenone derivative, (2-hydroxy-4-(3-methacryloxy-2-hydroxylpropoxy) benzophenone (BPMA) in acrylic resin. If ϵ is the molecular extinction coefficient (linked to the substance), the absorbed intensity I follows a law of the form:

$$I(x) = dF/dx = \epsilon \cdot c \cdot F_0 \cdot \exp(-\epsilon \cdot c \cdot x) = F_0/\mu \cdot \exp(-x/\mu) \quad (6)$$

where F_0 is the incident flux (assumed to be perpendicular to the layer to be polymerized), x the depth, and c the concentration of the initiator. The optical thickness, μ , is defined as the inverse of $\epsilon \cdot c$. μ is of the same order of magnitude as the polymerized thickness e (but $\mu > e$ for the layers to bond together) and depends on the wavelength (μ increases when the absorption coefficient decreases). It is thus not always possible to use a commercial resin with a 3D machine from another supplier which uses different concentrations of initiators and

wavelengths. It is on this principle that the stereolithography with one photon was developed in 1984: installation of a layer of photopolymerizable resin of thickness e , slightly lower than μ ; illumination solved on surface to polymerize precisely the zones to be transformed; installation of a new layer, etc., until the realization of a 3D object.

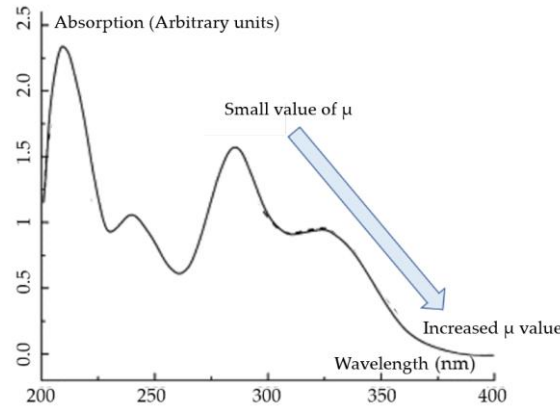


Figure 13. Absorption spectrum of a benzophenone derivative.

4.2.2. Absorption by a Filled Resin

Under conditions where light is the object of diffusion, the optical thickness decreases (even if, to a first approximation, the transmission of light energy follows a law close to the Beer–Lambert law [58,59]). This penetration thickness, E_p , is defined, in the absence of absorption by the resin, approximately by:

$$E_p = 2D_{50}/(3 \cdot Q \cdot C) \tag{7}$$

where the symbols represent the following:

- D_{50} : the average diameter of the particles (assumed to be spherical);
- Q : light scattering parameter defined by $h \cdot \Delta n^2 / \lambda$, with h the interparticle distance;
- λ : irradiation wavelength;
- Δn : the difference in refractive indexes between the resin and the mineral filler (with indexes that are of the order of 2) or organic;
- C : the charge density.

With the initiator, if μ is the optical thickness in the absence of filler, the thickness, μ_c , in the presence of solid additives is expressed by the following approximate relationship [2]:

$$1/\mu_c = 1/\mu + 1/E_p \tag{8}$$

In fact, from the calculation, perpendicularly to the layer the presence of fillers reduces the depth of polymerization and laterally increases it unless the powders used absorb the light (competition between absorption and diffusion of light).

4.2.3. Polymerized Depth

We have shown that T_1 can be expressed as:

$$T_1 = ((2kt/R_0)^{1/2})/kq \tag{9}$$

with R_0 the free radical production rate, which, under the conditions considered, becomes.

$$R_0 = \Phi \cdot (dF/dz) \cdot \exp(-z/\mu) = R_1 \cdot \exp(-z/\mu) \tag{10}$$

where z is the depth of the fluid, F the incident flux, and Φ is the quantum yield of free radical production.

For a time T very slightly higher than T_1 , the polymerization has started and the resin becomes solid. During this time, the polymerization reaction kinetics is (using the quasi-stationary states approximation):

$$d(R\cdot)/dt = -k_1 \cdot (R\cdot) \cdot (M) = d(M)/dt \quad (11)$$

where (M) is the monomer concentration.

Then, at least a reaction rate RR is stable (see Equation (12), assuming that (M) stays close to $(M)_0$); then, as a first approximation, the variation in monomer concentration $\Delta(M)$ is expressed by Equation (13). Thus, if the transformation is spatially isotropic, the transformed thickness varies substantially as $(\Delta(M))^{1/3}$ at least as long as the resin remains fluid.

$$RR = k_1 \cdot ((R_1 \cdot \exp(-z/\mu)/(2kt))^{1/2} \cdot (M)_0) \quad (12)$$

$$\Delta(M) = k_1 \cdot (R\cdot) \cdot (M)_0 \cdot (T - T_1) = k_1 \cdot ((R_1 \cdot \exp(-z/\mu)/(2kt))^{1/2} \cdot (M)_0 = K \cdot \exp(-z/2\mu) \quad (13)$$

where

$$K = k_1 \cdot ((R_1)/(2kt))^{1/2} \cdot (M)_0 \quad (14)$$

For a chain length of the order of 100, a molar mass of about 200 g for each monomer unit, and a heat capacity of $1.5 \text{ J} \cdot \text{g}^{-1} \cdot \text{°C}^{-1}$, the propagation reaction generates approximately $20 \text{ kJ} \cdot \text{M}^{-1}$ at each step related to the propagation process, i.e., a maximum increase in fluid temperature to about 70–80 °C (heat that dissipates rapidly by thermal diffusion). Several phenomena can modify this situation:

- The use of oligomers (reduction in chain length and increase in the molar mass of oligomeric units);
- The use of passive fillers, which reduces the phenomenon;
- The polymerization kinetics function of the resin;
- The heat transfer (Fourier law) from the reactive zones to the whole reactor.

Models show that the resolution can be less than one micrometer [14]. Moreover, for a flux density $F(0,r)$ of monochromatic light arriving on the resin surface, assuming a Gaussian beam (cylindrical symmetry), the local absorbed light intensity is defined by a law proportional to $\exp(-z/\mu)$, where μ is the optical thickness, which leads to a time T_1 before the reaction starts (cf. Figure 2). A Monte Carlo simulation with a Gaussian laser beam reaching the resin surface orthogonally, presented in Figure 14, illustrates the complex influence of the light exposure time on the shape of the polymerized zone in a one-photon process.

As a reminder, the distance μ corresponds to an attenuation of the light flux of $1/e$.

An important effect is that, after T_1 , the evolution of polymerization follows an apparent logarithmic law as a function of the irradiation time, which leaves some “slack” in the choice of the polymerization time, as long as the inhibitors have been used up.

4.3. Simultaneously Absorbed Two-Photon Stereolithography

4.3.1. General Framework

When we are able to increase F today, with femtosecond pulse lasers, in the expression

$$dF/dx = -\alpha \times F - \beta F^2 - \gamma F^3 - \dots \quad (15)$$

it is the second term, F^2 , that can become dominant. The two-photon absorption shown in Figure 12 (right) corresponds to the simultaneous absorption of two photons of identical or different frequencies leading to the promotion, in a single step, of a molecule from a ground state to an electronically excited state. The energy difference between these two states is equal to the sum of the energies carried by the two photons. Two-photon absorption is

a third-order process, different from classical absorption, because it is proportional to the square of the intensity of the incident light, which makes it a nonlinear optical process.

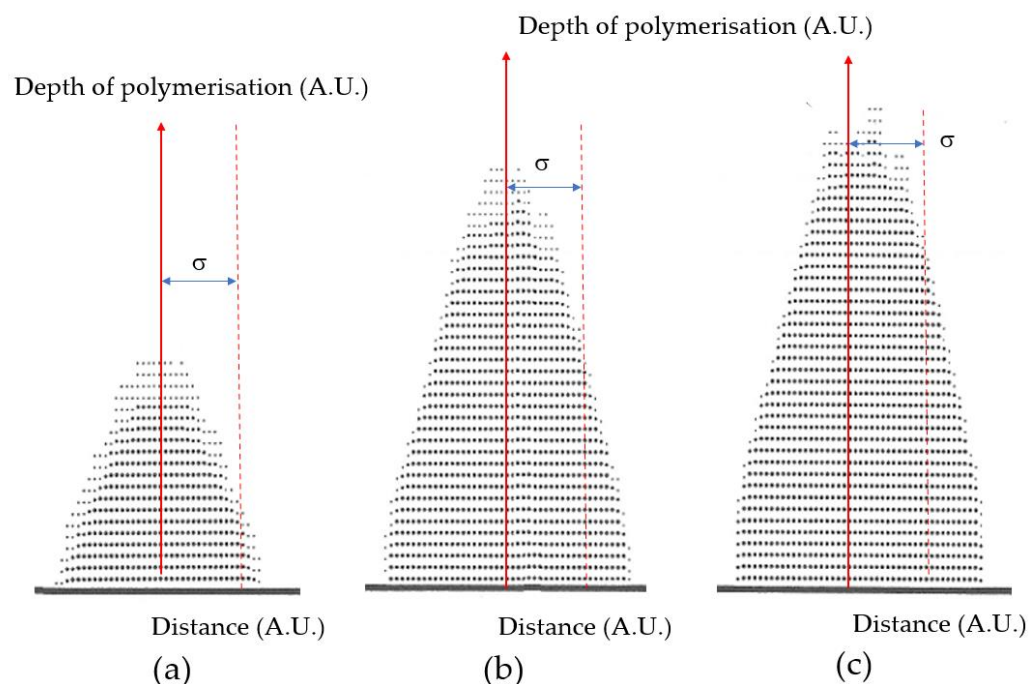


Figure 14. Polymerization of a monomer by radical reaction (a: 50,000 shots, b: 1,000,000, c: 750,000) using one-photon electron excitation: increase in polymerization depth (arbitrary units—A.U.) versus time, and σ the width of the Gaussian at half height.

4.3.2. Resolution

If we consider a two-photon process, it is because the associated nonlinear system will result in a better spatial resolution than that of the incident beam (significantly lower than the square of the radial power density because the threshold of consumption of the inhibitors must always be exceeded, as shown in Figure 4). In order to excite an initiator molecule by a two-photon pathway, the photons must be spatially and temporally concentrated (remember that in a vacuum, light travels 0.3 mm in one picosecond (i.e., about 0.2 mm in the resin); it is therefore necessary to pay attention to the different optical paths involved, some of which may constitute delay lines). It is from this excited state that the unstable species, responsible for the polymerization, will be produced during a dissociative chemical process. Consequently, one cannot normally use a continuous laser but one or more lasers with very short pulse durations (picosecond or better femtosecond). Indeed, by “compressing” the photons spatially and temporally, the probability of two-photon excitation is “obviously” increased. This type of illumination also has the consequence that the excitation is generally confined to the immediate vicinity of the focal point of a concentrated beam (which is what is sought). Figure 15 presents qualitatively the gain in spatial resolution, as a function of the square of the flux density represented in this figure by the red curve.

The writing of two adjacent exposures allows the estimation of the resolution: the quantities of molecules excited locally to, below a certain minimum distance, form a single polymerized set. Beyond that, there is a separation into two distinct volumes. This transition is related to the two-photon Sparrow criterion (this criterion means that for a lens with numerical aperture (NA) of 1.4, the minimum lateral separation is about one quarter of the free-space wavelength, $\lambda/4$). For example, the separation between the two voxels must be 100 nm for $\lambda = 400$ nm.

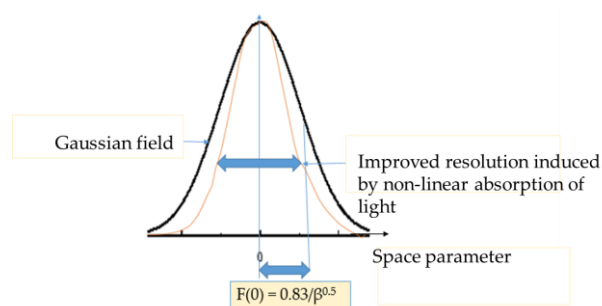


Figure 15. Spatial resolution gain induced by two-photon absorption process.

With τ the duration of a pulse, T the repetition frequency, and P_{mean} the average power, if $T = 80$ MHz, $P_{\text{mean}} = 3$ W, and $\tau = 140 \times 10^{-15}$ s, we obtain for the peak power a value $P_{\text{peak}} = 1.7 \times 10^6$ W, which corresponds to the range where two-photon absorption can lead to electronic excitation of the initiator. These approximate data define the framework of one of the constraints to be satisfied so that there is a possibility of two photon absorption.

Figure 16 illustrates one of the interests of simultaneously absorbed two-photon stereolithography in terms of spatial resolution (inspired by [60]; see also [61]).

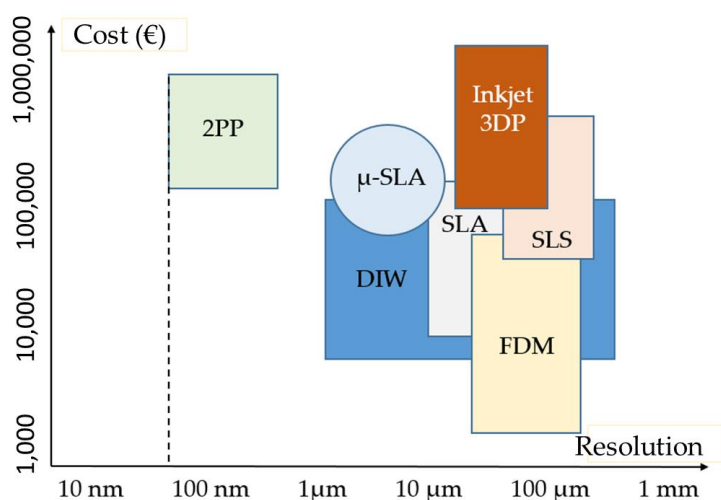


Figure 16. 3D machine approximative cost/resolution relationships. 2PP: two-photon stereolithography; SLA: single-photon stereolithography; μ -SLA: μ -mask stereolithography [62]; DIW: direct writing; Inkjet 3DP: direct injection molding; SLS: selective laser sintering; FDM: molten filament deposition.

4.3.3. Classical Initiators

Kannan et al. [63] and Belfield et al. [64] give examples of calculated values for β from experimental data of biphoton absorption coefficients. According to Selimis et al. [65], the molecules with good biphoton absorption efficiency are classically the compounds of the benzophenone family [66]. In addition to the data of Schafer et al. [67], data on other substances have been published [68–78]; these are essentially chemical compounds containing aromatic ketone groups that are known to have the potential to form, with good quantum yield, free radicals that can initiate radical polymerization chain reactions [2].

4.3.4. Two-Photon μ -Stereolithography

Considering the potential resolution of less than a micrometer, the difficulty of producing layers in stereolithography under these conditions, and the existence of pulsed lasers at “reasonable” costs, this two-photon absorption principle has already been adopted for the production of very small objects. The beam is focused at the point of initiation, followed by polymerization. The displacement in space of the support (or, in a reciprocal way, the laser

beam) allows, without the reactive fluid moving, the realization of an object from near to near. Figure 17 illustrates the principle of this micro-fabrication.

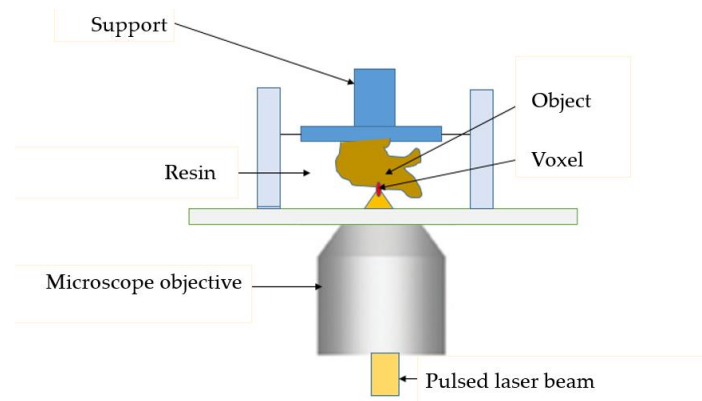


Figure 17. Principle of the two-photon stereolithography setup.

According to [79–83], by using multi-photon absorption, excellent resolution can be achieved, as shown in Figure 18. The technology is developing [39,76–85], with a few manufacturers occupying the market (e.g., Micro-light—<http://www.microlight.fr/TPP.html>, accessed on 22 March 2023; Up-Nano—<https://www.upnano.at/technology/#scale-applications>, accessed on 22 March 2023; Nano-Scribe—<https://www.nanoscribe.com/en/>, accessed on 22 March 2023). Application targets include biology, nano-photonics and μ -actuators, μ -fluidics, neural electronics, and heterogeneous integration.

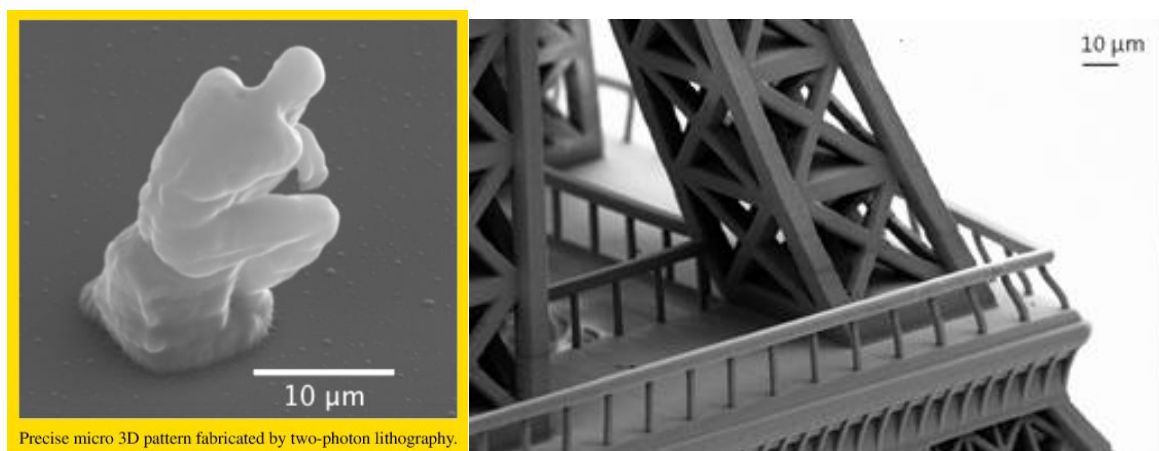


Figure 18. Multi-photon micro-stereolithography (left: sculpture according to Park et al. [79]; right: Eiffel Tower element according to Ovsianikov et al. [82]).

4.3.5. Two-Photon Stereolithography

Three-dimensional printing by one-photon photopolymerization transforms a liquid resin into a solid material [2]. There are two phenomena to consider: first, the addition (already at the scanning stage) of support pillars of the object under construction is necessary to ensure the smooth printing process of parts with complex shapes. Second, The removal of the supports, usually by hand, is a time-consuming process. Moreover, the realization of very thin layers is generally delicate (cf. μ -stereolithography) and consequently, developing 3D printing by photopolymerization without support is a research direction which can lead to relevant advantages.

Proof of Concept

With a long working distance microscope objective (focal length 4 mm, numerical aperture 0.42, working distance 20.5 mm), an average power of 15 mW at 515 nm, pulse

duration of 500 fs, and a 1 kHz repetition rate, a proof of concept was performed by polymerizing an acrylic resin, HDDA (1,6-Hexanediol diacrylate), in a spectroscopic cell (see Figure 11). In a first step, the beam focal point is placed at the exit surface of the small reservoir so as to be able to hang a horizontal beam in a second step. Taking into account the characteristics of the beam and the objective, the diameter of the beam at the focal plane is estimated at about ten micrometers (the diffraction limit with this objective is about $1\ \mu\text{m}$ in air). In a second step, the tank is moved so that the focal point approaches the entrance face (cf. Figure 19 highlighting the 6 mm long object thus created); finally, in a third step, the beam is moved along a vertical line, allowing the fabrication of a bayonet-shaped physical object (1.3 cm high).



Figure 19. Proof of concept (the lens of on the left part of the figure).

This demonstrates the possibility of reaching dimensions corresponding to the main 3D market. This simple proof of concept could be used to go further and make applicable parts.

Removal of Layers

Since there can be a volume change related to the polymerisation [2], the part being built should preferentially be supported to prevent it from being deformed by its gravitational fall (Stokes' law). This effect can be notably limited by increasing the viscosity of the resin (which is not a problem since we are working without a layer by layer process), or by adding various fillers to the resin (but which keep the medium transparent to the laser wavelength) that will make the medium practically solid or with solid behavior. Figure 20 gives an example of a realization of a 3D part in a solid reactive medium [86–89]. The rather classical setup is shown on the right-hand side of the figure (see [90]).

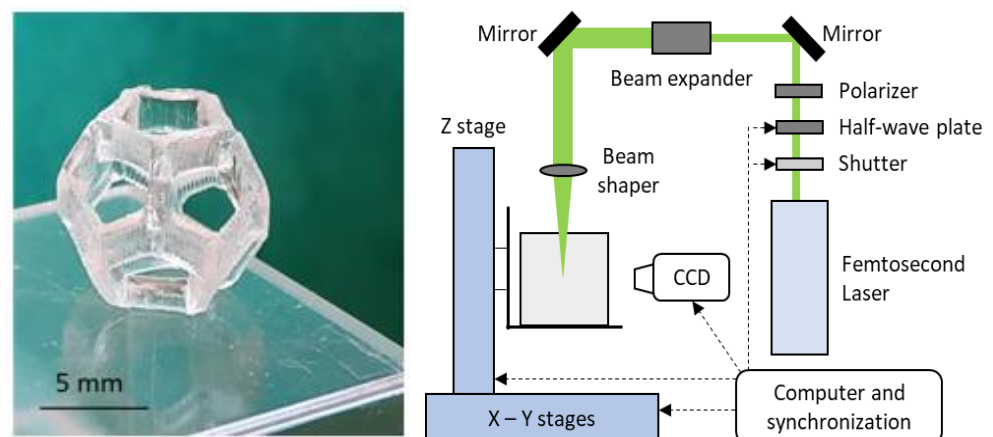


Figure 20. Part (realized without layer and without support) and two-photon 3D device [91].

In these experiments, we used conventional photochemical initiators (those used for one-photon polymerizations) and standard acrylic resins with known polymerization kinetics after free radical production [2].

Voxels Size vs. Time

By focusing the laser beam inside the reactive fluid, the initiator is excited by biphotonic absorption and leads to polymerization. Depending on the local flux density, the curve of Figure 2 is followed: no polymerization reaction as long as the inhibitors are not consumed (zone I); then, beginning of polymerization with a fluid material at the beginning which becomes pasty (zone II), before a hardening phase (zone III). To study the relationship between the concentration of the initiator, the luminous flux, and the size of a voxel, a device where we produce a very elongated ellipsoid was chosen to have the best accuracy of measurement of the long axis of the voxel, by taking out the voxel with a small clamp, the short axis can be partially degraded. Indeed, as shown schematically in Figure 21, the voxel is made of resin whose reactional progress in the course of transformation is variable. There is therefore a fragile zone that should not be degraded before washing for the measurement of the long axis [3].

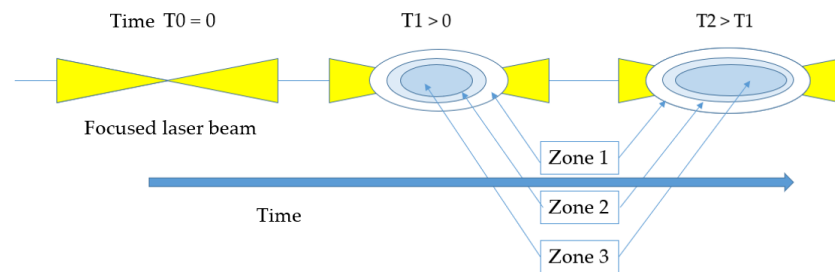


Figure 21. Two-photon polymerization as a function of time.

In this simplified approach, the flux density is, within a multiplicative factor λ , of the form $F_0/\text{length } L^2$ in the beam direction, with $T1$ defined by $T1 = ((2kt/R_0)^{1/2})/kq$. Under the conditions of Figure 21, on the one hand, $T1$ is proportional to $((1/R_0)^{1/4})$ since it is a two-photon absorption and, on the other hand, to the inverse of the concentration of the initiator. On this basis, all other things being equal, it is possible to relate the length of the voxel with the irradiation time. These experiments were conducted with different laser powers and are shown in Figure 22.

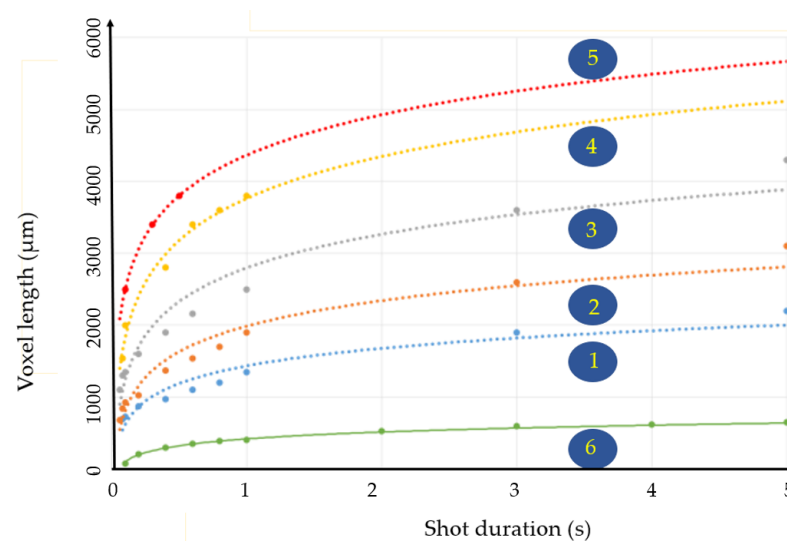


Figure 22. Voxel length vs. irradiation time (sum of the different laser pulses). Laser 1 (500 fs, 515 nm, 1 kHz): 2.3 mW; 2: 5.4 mW; 3: 10 mW; 4: 20 mW; 5: 38.5 mW. Laser 2 (500 ps, 532 nm, 1 kHz): 40 mW.

In order to optimize the production of an object using this two-photon absorption method, we have tried to model the variations in the voxel length vs. the number of shots (or time) and the power of the source, knowing that the absorbed light is proportional to the number of shots (or to the concentration of the initiator (irgacure)) and to the square of the luminous flux, and that this luminous flux is approximately proportional to the inverse of the distance to the focal plane.

However, it is the polymerization reaction mechanism that leads to the S-curve in Figure 2 that poses a problem for simplified and operational modeling. Indeed, it is only after the disappearance of the inhibitor (dissolved oxygen and a stabilizer based on hydroquinone or its family) that the polymerization reaction begins; in fluid media, it starts with a chain reaction whose kinetics depend on the square root of the light absorption rate, and then changes to a proportionality with this last parameter [2].

As a reminder, in zone (I), between 0 and T1 there is no reaction ($T1 = Q/Ia$); in zone (II), the kinetics starts at $Ia^{1/2}$ then evolves towards a proportionality to Ia because of the rheological change induced by the photochemical cross-linking; in zone (III), we consider for simplicity that the reaction is blocked.

In addition, in these considerations there are a number of assumptions that should be validated, such as the stability of Ia, which assumes the non-consumption of the initiator, and non-knowledge, such as the values of the rate constants, the concentrations of the inhibitors, the concentration of M over time, etc. For all these reasons, it was not possible to consider a model other than phenomenologically linking some main parameters in order to optimize the fabrication of objects by the two-photon process which is the subject of this work.

Based on this, and as an illustration of the control of voxel size as a function of femtosecond laser power, Figure 23 shows the phenomenological relationship defined by a classical kinetic model of free radical polymerization adapted to the two-photon initiation process (cf. [2,60,92,93]). This type of figure illustrates the possibility of controlling the relationship between the incident flux and the voxel size.

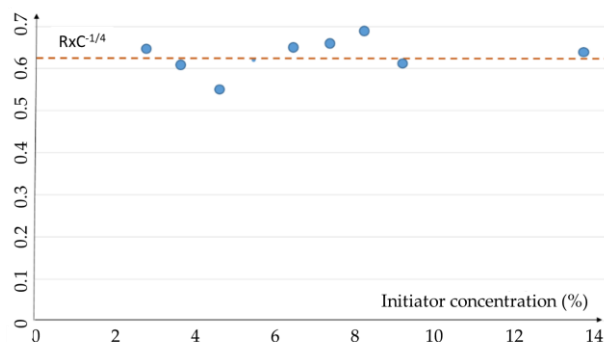


Figure 23. Relation $R \cdot C^{-1/4}$ vs. C (average power 38.5 mW in the infrared)—R is the longest axis of the voxel (ellipsoid shape) and C the concentration of the initiator—exposure time is 10 s.

Figure 24 shows the effect of this experimental law on the length of the voxel for all the measurements presented in Figure 23. Given the difficulty of measuring the value of the length (presence of “soft” material around the hard material), it is possible to express all the experimental data by a simple law, which is:

$$L = \alpha \cdot t \cdot C^{1/4} \tag{16}$$

where α is a fitting parameter, t represents the irradiation time (number of shots), and C is the initiator concentration.

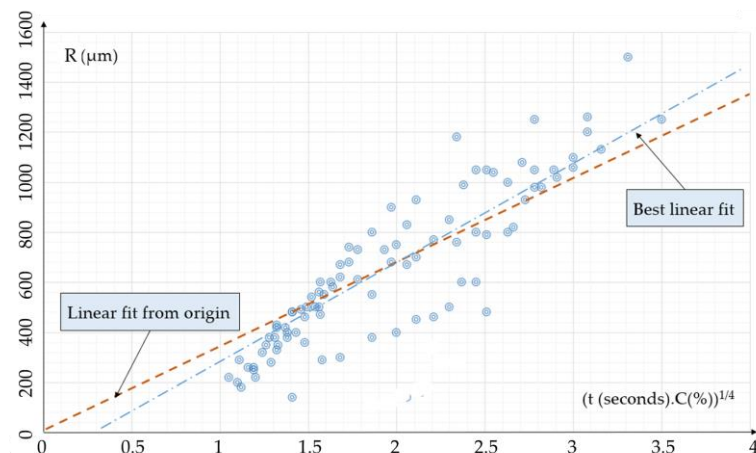


Figure 24. Variations in R vs. $t \cdot C^{1/4}$.

This approximate knowledge allows the estimation of the voxel size desired by the designer of an object, the adequate polymerization time for a voxel, and thus to realize the object.

Interest of Loaded Resins

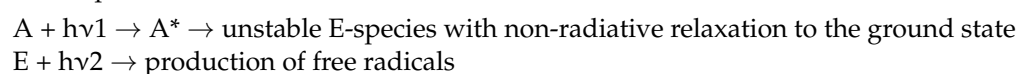
In agreement with [94], fillers such as silica in nanoparticle form can be added to organic compounds such as acrylic resins without affecting the transparency of the medium. This possibility allows, in principle, very high viscosities to be reached. However, photochemical polymerizations are generally subject to volume shrinkage. In the absence of support, the object changes position. By preventing it from moving, it is possible to produce objects without layers and without support from a polymer containing silica (nano-silica of 20 nm median diameter). After de-binding and sintering, it is thus possible to produce sequentially, after removal of the organic material, transparent silica objects [91,95]. Figure 25 shows a convincing result (probably not applicable to all other forms of nanoparticulate fillers that do not allow a transparent reactive medium to be obtained).



Figure 25. Silica part after de-binding and sintering [91].

4.4. Two-Photon Stereolithography, Sequential Absorption

As presented in Section 4.1, the principle of such an initiation possibility is based on the following kinetic mechanism, where A is a molecule excitable at the frequency λ_1 from a laser plane:



This principle is exploited by Xolo GmbH [96] by realizing a laser plane at ν_1 with an A^* species whose lifetime is sufficient for a displacement of the light excitation (at 90°) to produce the free radicals necessary for the creation of a 3D object. We move the laser sheet (equivalent to layers) and, step by step, we create the object. It is thus a question of controlling the distribution of the power density in the sheet, the time between the production of A^* , and the irradiation at ν_2 .

4.5. Conclusions

It is shown that one- and two-photon absorption processes (simultaneous and sequential) can lead to the effective realization of 3D objects by stereolithography. The space covered goes from micrometers to a few centimeters (transparency of the reactive fluid), or rarely decimeter (time of setting of the layers). These different results are related to the power of the light sources, the wavelength, the quantum yield of free radical formation, the nature of the reactive fluid, etc., but above all they are associated with the local light intensity, which defines the voxels involved in the realization of the 3D objects. This knowledge is able to optimize a 3D manufacturing process.

5. General Conclusions

This paper, based on stereolithography, has first of all allowed us to recall some important parameters, now classical, such as the voxel, but also printability, etc. However, the central point of interest of the document is to show that the designer can play on the modes of interaction of light-reactive matter with conventional resins (except for a process with sequential biphotonic excitation, more complex from a chemical point of view). In this context, continuous or pulsed sources can be envisaged, the latter allowing us to consider manufacturing without passing through the stage of a layer-by-layer process and the manufacture of “green” parts which can be transformed into glass. The control of these interactions allows an optimized management of a manufacturing process.

This field, where polymerization initiation is particular and which allows excellent spatial resolution, must meet several development challenges, which is also partly true for stereolithography in general:

- To be able to manufacture ever finer structures (in reasonable manufacturing times);
- To have a fast means of displacement of the laser beam(s) without prejudice to the resolution, keeping the optical properties of the light beams;
- To have a good transparency of polymerizable materials (with commercial resin, it becomes difficult to manufacture an object beyond a few cm (typically 5 for parts of 10));
- To be able to go beyond polymer parts; the example of silica, transparent charge, illustrates the direction of work to be carried out as long as one has a transparent reactive set;
- To have less expensive laser sources;
- Considering multi-material manufacturing and approaching the 4D technologies that are emerging.

It is indubitable from the positive work undertaken on these themes that industrial activities on the manufacture of decimeter-sized objects could emerge, but the road is undoubtedly still long for two-photon stereolithography. However, it should be remembered that, today, more than a thousand users worldwide are using two-photon 3D manufacturing technology to produce microscale objects that previously seemed difficult or even impossible to manufacture, while relying on very similar concepts. However, this approach is competing with other sequential single- or two-photon processes [97].

In recent years, the creativity of researchers has led to the emergence of new processes where light is involved. This means that the stabilization of these processes is not yet envisaged. No doubt in the future we will be offered very original operational photonic systems, such as the one from Xolo GmbH [96].

Author Contributions: Conceptualization, J.-C.A.; methodology, J.-C.A. and L.G.; investigation, T.D.; writing—original draft preparation, J.-C.A.; writing—review and editing, L.G.; supervision, J.-C.A.; project administration, L.G.; funding acquisition, L.G. and J.-C.A. All authors have read and agreed to the published version of the manuscript.

Funding: This research received funding by SATT Sud-Est—France.

Institutional Review Board Statement: Not applicable.

Informed Consent Statement: Not applicable.

Data Availability Statement: The data presented in this study are available on request from the corresponding author.

Conflicts of Interest: The authors declare no conflict of interest.

References

1. André, J.C.; Le Méhauté, A.; De Witte, O. Dispositif pour Réaliser un Modèle de Pièce Industrielle. French Patent 84 11 241, 16 July 1984.
2. André, J.C. *From Additive Manufacturing to 3D/4D Printing—Volume 1: From the First Concept to the Present Applications. Volume 2: Improvement of the Present Technologies and Constraints. Volume 3: Breakdown Innovations: Programmable Matter. 4D Printing and Bio-Printing*; ISTE/Wiley: London, UK, 2017.
3. Bougdid, Y.; Maouli, I.; Rahmouni, A.; Mochizuki, K.; Bennani, I.; Halim, M.; Sekkat, Z. Systematic $\lambda/21$ resolution achieved in nanofabrication by two-photon-absorption induced polymerization. *J. Micromech. Microeng.* **2019**, *29*, 035018. [CrossRef]
4. Susperrgui, N. Etude Théorique de la Polymérisation D'esters par Voie Organométallique et Organique. Ph.D. Thesis, Université de Toulouse, Toulouse, France, 2010.
5. Fiedor, P.; Pilch, M.; Szymaszek, P.; Chachaj-Brekiesz, A.; Galek, M.; Ortyl, J. Photochemical Study of a New Bimolecular Photo-initiating System for Vat Photopolymerization 3D Printing Techniques under Visible Light. *Catalysts* **2020**, *10*, 284. [CrossRef]
6. Sertoglou, K. 3D Systems Announces Two New SLA 750 3D Printers, Resin and More—Technical Specifications and Pricing. Available online: <https://3dprintingindustry.com/news/3d-systems-announces-two-new-sla-750-3d-printers-resin-and-more-technical-specifications-and-pricing-207277/> (accessed on 27 May 2023).
7. Stevenson, K. Ten Juicy 3D Print Corporate Acquisition Targets. Available online: <https://commentclient-com.ngontinh24.com/article/ten-juicy-3d-print-corporate-acquisition-targets-fabbaloo> (accessed on 27 May 2023).
8. Mélanie, W. Quels Sont les Matériaux Innovants du Formnext 2021? Available online: <https://www.3dnatives.com/materiaux-formnext-2021/> (accessed on 27 May 2023).
9. Mélanie, W. Quel Procédé faut-il Privilégier? Nous Avons Interrogé 3 Experts Français du Secteur afin d'en Savoir Plus! Available online: <https://www.3dnatives.com/conseils-experts-imprimante-3d-resine-24082021/> (accessed on 27 May 2023).
10. Merck "Irgacure". Available online: <https://www.sigmaaldrich.com/FR/fr/search/irgacure?focus=products&page=1&perpage=30&sort=relevance&term=irgacure&type=product> (accessed on 27 May 2023).
11. von Raumer, M.; Suppan, P.; Jacques, P. Photoinduced charge transfer processes of triplet benzophenone in acetonitrile. *J. Photochem. Photobiol. A Chem.* **1997**, *105*, 21–28. [CrossRef]
12. Sigma-Aldrich "AIBN". Available online: [https://www.sigmaaldrich.com/FR/fr/search/azobisisobutyronitrile-\(aibn?focus=products&page=1&perpage=30&sort=relevance&term=azobisisobutyronitrile%20\(aibn&type=product](https://www.sigmaaldrich.com/FR/fr/search/azobisisobutyronitrile-(aibn?focus=products&page=1&perpage=30&sort=relevance&term=azobisisobutyronitrile%20(aibn&type=product) (accessed on 27 May 2023).
13. Sigma-Aldrich "Benzoyl Peroxide". Available online: https://www.sigmaaldrich.com/FR/fr/search/94-36-0?focus=products&gclid=EAIaIQobChMI3_6Czv-6_gIVZxMGAB12xwGCEAMYASAAEgKBLfD_BwE&page=1&perpage=30&sort=relevance&term=94-36-0&type=cas_number (accessed on 27 May 2023).
14. André, J.C.; Corbel, S. *Stéréo-Photolithographie Laser*; Polytechnica: Paris, France, 1994.
15. Irmouli, Y.; George, B.; Merlin, A. Study of the polymerization of acrylic resins by photo-calorimetry: Interactions between UV initiators and absorbers. *J. Therm. Anal. Calorim.* **2009**, *96*, 911–916. [CrossRef]
16. Nuyken, O.; Pask, S.D. Ring-Opening Polymerization—An Introductory Review. *Polymers* **2013**, *5*, 361–403. [CrossRef]
17. Wang, X.; Jiang, M.; Zhou, Z.W.; Gou, J.H.; Hui, D. 3D printing of polymer matrix composites: A review and prospective. *Compos. Part B Eng.* **2017**, *110*, 442–458. [CrossRef]
18. Charton, N.; Felderman, A.; Theis, A.; Stenzel, M.H.; Davis, T.P.; Bamer-Kowolik, C. Initiation efficiency of 2,2'-azo-bis-(isobutyronitrile) in bulk dodecyl acrylate free radical polymerization over a wide conversion and molecular weight range. *J. Polym. Sci.* **2004**, *42*, 5170–5179. [CrossRef]
19. Makitra, R.G.; Polyuzhin, I.P.; Golovata, I.P. Effect of solvation on the decomposition rate of azo-di-iso-butyro-nitrile. *Russ. J. Gen. Chem.* **2005**, *75*, 172–176. [CrossRef]
20. Guo, S.; Wan, W.; Chen, C.; Chen, W.H. Thermal decomposition kinetic evaluation and its thermal hazards prediction of AIBN. *J. Therm. Anal. Calorim.* **2013**, *113*, 1169–1176. [CrossRef]
21. Lee, M.H.; Chen, J.R.; Shine, G.Y.; Shu, C.M. Simulation approach to benzoyl peroxide decomposition kinetics by thermal calorimetric methods. *J. Taiwan Inst. Chem. Eng.* **2014**, *45*, 115–120. [CrossRef]
22. Odian, G. *Radical Chain Polymerization in Principles of Polymerization*; J. Wiley&Sons: New York, NY, USA, 2004.
23. André, J.C.; Grisoni, B.; Corbet, A. Dispositif de Réalisation d'objets Réels par Polymérisation Induite Thermiquement. French Patent 86 023 27, 20 February 1986.
24. Corbel, S.; Grisoni, B.; Jezequel, J.Y.; Andre, J.C. Morpho-synthesis by space resolved thermal polymerization induced by IR lasers. *Can. J. Chem. Eng.* **1992**, *70*, 1041–1047. [CrossRef]
25. Kompis, V. (Ed.) *Composites with Micro- and Nano-Structure—Computational Modeling and Experiments*; Springer: Frankfurt, Germany, 2007.

26. Le Duigou, A.; Chabaud, G.; Castro, M. Impression 3D/4D de matériaux composites thermoplastiques. *Tech. L'ingénieur* **2021**, BM7922. Available online: <https://www.techniques-ingenieur.fr/base-documentaire/materiaux-th11/finitions-des-plastiques-fabrication-additive-des-polymeres-42475210/impresion-3d-4d-de-materiaux-composites-thermoplastiques-bm7922/> (accessed on 27 May 2023). [CrossRef]
27. Aguiar, B.A.; Nisar, A.; Thomas, T.; Zhang, C.; Agarwal, A. In-situ resource utilization of lunar highlands regolith via additive manufacturing using digital light processing. *Ceram. Int.* **2023**, *49*, 17283–17295. [CrossRef]
28. Mollon, G. A numerical framework for discrete modelling of friction and wear using Voronoi polyhedrons. *Tribol. Int.* **2015**, *90*, 343–355. [CrossRef]
29. Enferad, S.; Petit, J.; Gaiani, C.; Falk, V.; Burgain, J.; De Richter, S.K.; Jenny, M. Effect of particle size and formulation on powder rheology. *Part. Sci. Technol.* **2020**, *39*, 362–370. [CrossRef]
30. Enferad, S. Compacting and Aging of Powders: Influence of the Formulation. PhD Thesis, Université de Lorraine, Lorraine, France, 2020.
31. Keller, S.; Jaeger, H.M. Aleatory architectures. *Granul. Matter* **2016**, *18*, 26. [CrossRef]
32. Ouabbas, Y.; Galet, L.; Patry, S.; Devrient, L. Modification des propriétés des poudres par enrobage à sec dans un mélangeur Cyclomix. In *Formulation des Solides Divisés*; EDP Sciences: Les Ulis, France, 2009.
33. Paroissien, E. Contribution Aux Assemblages Hybrides (Boulonnés/Collés)—Application Aux Jonctions Aéronautiques. Ph.D. Thesis, ENSMP, Paris, France, 2016.
34. Bretton, C.; Villoutreix, G. Familles d'adhésifs et caractérisation d'un collage structural. *Tech. L'ingénieur* **2022**, AM3560 V2. Available online: <https://www.techniques-ingenieur.fr/base-documentaire/materiaux-th11/applications-des-plastiques-42141210/familles-d-adhesifs-et-caracterisation-d-un-collage-structural-am3560/> (accessed on 27 May 2023). [CrossRef]
35. Schaeffer, P.; Bertsch, A.; Corbel, S.; Jezequel, J.Y.; Andre, J.C. Industrial photochemistry: XXIV—Relations between light flux and polymerized depth in laser stereo-photolithography. *J. Photochem. Photobiol. A Chem.* **1997**, *107*, 283–290. [CrossRef]
36. Göppert-Mayer, M. Historic Article—Elementary processes with two quantum transitions. *Ann. Für Phys.* **2009**, *18*, 466–479. [CrossRef]
37. Adamson, A.W.; Lewis, J.D. Method and Apparatus for Generating 3 Dimensional Patterns. U.S. Patent 3609706 A, 6 December 1968.
38. McGinniss, V.D.; Schwerzel, R.E. Photo-Polymerizable Composition Containing a Photosensitizer Donor and Photo-Initiator Acceptor. U.S. Patent 4571377 A, 23 February 1984.
39. Jiang, L.J.; Zhou, Y.S.; Xiang, W.; Gao, Y.; Huang, X.; Jiang, L.; Balocchini, T.; Silvain, J.F. Two photon polymerization: Investigation of chemical and mechanical properties of resin using Raman micro-spectroscopy. *Opt. Lett.* **2014**, *39*, 3034–3037. [CrossRef]
40. Wei, J.; Li, Y.; Song, P.; Yang, Y.; Ma, F. Effect of Polymerization on the Charge-Transfer Mechanism in the One (Two)—Photon Absorption Process of D–A-Type Triphenylamine Derivatives. *J. Phys. Chem.* **2021**, *A125*, 777–794. [CrossRef] [PubMed]
41. McClain, W.M. Two-photon molecular spectroscopy. *Acc. Chem. Res.* **1974**, *7*, 129–135. [CrossRef]
42. Cagnac, B.; Grynberg, G.; Biraben, F. Spectroscopie d'absorption multi-photonique sans effet Doppler. *J. Phys.* **1973**, *34*, 845–858. [CrossRef]
43. Bonin, K.D.; McIlrath, T.J. Two-photon electric-dipole selection rules. *J. Opt. Soc. Am.* **1983**, *B1*, 52–55. [CrossRef]
44. Melikechi, N.; Allen, L. Two-photon electric-dipole selection rules and nondegenerate real intermediate states. *J. Opt. Soc. Am. B* **1986**, *3*, 41–44. [CrossRef]
45. Dufour, P.; Dufour, S.; Castonguay, A.; McCarthy, N.; De Koninck, Y. Two-photon laser scanning fluorescence microscopy for functional cellular imaging: Advantages and challenges or One photon is good . . . but two is better! *Med. Sci.* **2006**, *22*, 837–844.
46. Lewandowska-Andralojc, A.; Hug, G.L.; Hörner, G.; Pedzinski, T.; Marciniak, B. Unusual photo-behaviour of benzophenone triplets in hexa-fluoro-isopropanol. Inversion of the triplet character of benzophenone. *J. Photochem. Photobiol.* **2012**, *244A*, 1–8. [CrossRef]
47. Kellmann, A.; Tfibel, F. Radicals produced from the laser-induced photoionization of acridine in solution. *J. Photochem.* **1982**, *18*, 81–88. [CrossRef]
48. Bensasson, R.; Land, E.J. Triplet-triplet extinction coefficients via energy transfer. *Trans. Faraday Soc.* **1971**, *67*, 1904–1915. [CrossRef]
49. Bagdasaryan, K.S.; Kirjukhin, Y.I.; Sinitsina, Z.A. Quantitative studies of bi-photonic reactions. *J. Photochem.* **1972**, *1*, 225–240. [CrossRef]
50. Nielsen, B.R.; Jørgensen, K.; Skibsted, L.H. Triplet—Triplet extinction coefficients, rate constants of triplet decay and rate constant of anthracene triplet sensitization by laser flash photolysis of astaxanthin, β -carotene, canthaxanthin and zeaxanthin in deaerated toluene at 298 K. *J. Photochem. Photobiol. A Chem.* **1998**, *112*, 127–133. [CrossRef]
51. Brinen, J.; Innes, J.; Kazan, J. T-T' absorption of molecules with extremely high extinction coefficients. *Chem. Phys. Lett.* **1972**, *15*, 69–72. [CrossRef]
52. Malval, J.P.; Dietlin, C.; Allonas, X.; Fouassier, J.P. Sterically tuned photo-reactivity of an aromatic α -diketones family. *J. Photochem. Photobiol.* **2007**, *A192*, 66–73. [CrossRef]
53. Malval, J.-P.; Jin, M.; Morlet-Savary, F.; Chaumeil, H.; Defoin, A.; Soppera, O.; Scheul, T.; Bouriau, M.; Baldeck, P.L. Enhancement of the Two-Photon Initiating Efficiency of a Thioxanthone Derivative through a Chevron-Shaped Architecture. *Chem. Mater.* **2011**, *23*, 3411–3420. [CrossRef]
54. Singh-Rachford, T.N.; Castellano, F.N. Low power visible to UV up-conversion. *J. Phys. Chem.* **2009**, *A113*, 5912–5917. [CrossRef]

55. Land, E.J. Extinction coefficients of triplet-triplet transitions. *Proc. R. Soc.* **1968**, *A305*, 457–471.
56. Almgren, M. The natural phosphorescence lifetime of biacetyl and Benzil in fluid solution. *Photochem. Photobiol.* **1967**, *6*, 829–840. [[CrossRef](#)]
57. Zhao, Y.; Dan, Y. Synthesis and characterization of a polymerizable benzophenone derivative and its application in styrenic polymers as UV-stabilizer. *Eur. Polym. J.* **2007**, *43*, 4541–4551. [[CrossRef](#)]
58. Bolland, D.; Gukllard, R.; Andre, J.; Guillard, R. Experimental Studies and Modelling of Light Distribution in Photopolymerizable Composite Materials. *Dent. Mater. J.* **1984**, *3*, 93–98. [[CrossRef](#)]
59. Braun, C.; Andre, J. Industrial photochemistry VII: Light distribution in a diffusing medium of titanium dioxide in water. *J. Photochem.* **1985**, *28*, 13–29. [[CrossRef](#)]
60. Zhakeyev, A.; Zhang, L.; Xuan, J. Photoactive resin formulations and composites for optical 3D and 4D printing of functional materials and devices. In *3D and 4D Printing of Polymer Nano-Composite Materials—Processes—Applications and Challenges*; Sadavisuni, K.K., Deshmukh, K., Almaadeed, M.A., Eds.; Elsevier: Amsterdam, The Netherlands, 2020; pp. 387–425.
61. Quan, H.; Zhang, T.; Xu, H.; Luo, S.; Nie, J.; Zhu, X. Photo-curing 3D printing technique and its challenges. *Bioact. Mater.* **2020**, *5*, 110–115. [[CrossRef](#)] [[PubMed](#)]
62. Bertsch, A.; Renaud, P. Micro-stereolithography. In *Stereolithography—Materials, Processes and Applications*; Bartolo, P.J., Ed.; Springer: New York, NY, USA, 2011.
63. Kannan, R.; He, G.S.; Yuan, L.; Xu, F.; Prasad, P.N.; Dombroskie, A.G.; Reinhardt, B.A.; Baur, J.W.; Vaia, R.A.; Tan, L.S. Diphenyl-amino-fluorene-based two-photon-absorbing chromophores with various π -electron acceptors. *Chem. Mater.* **2001**, *13*, 1896–1904. [[CrossRef](#)]
64. Belfield, K.D.; Schafer, K.J.; Liu, Y.; Liu, J.; Ren, X.; Stryland, E.W.V. Multiphoton-absorbing organic materials for microfabrication. emerging optical applications and non-destructive three-dimensional imaging. *J. Phys. Org. Chem.* **2000**, *13*, 837–849. [[CrossRef](#)]
65. Selimis, A.; Mironov, V.; Farsari, M. Direct laser writing: Principles and materials for scaffold 3D printing. *Microelectron. Eng.* **2015**, *132*, 83–89. [[CrossRef](#)]
66. Woodward, J.R.; Lin, T.S.; Sakaguchi, Y.; Hayashi, H. Biphotonic photochemistry of benzophenone in DMSO: A flash photolysis EPR study. *Mol. Phys.* **2002**, *100*, 1235–1244. [[CrossRef](#)]
67. Schafer, K.J.; Hales, J.M.; Balu, M.; Belfield, K.D.; Van Stryland, E.W.; Hagan, D.J. Two-photon absorption cross-sections of common photo-initiators. *J. Photochem. Photobiol.* **2004**, *A162*, 497–502. [[CrossRef](#)]
68. Kim, H.M.; Cho, B.R. Two photon materials with large two-photon cross section: Structure property relationship. *Chem. Commun.* **2009**, 153–164. [[CrossRef](#)]
69. Devi, C.L.; Yesudas, K.; Makarov, N.S.; Rao, V.J.; Bhanuprakash, K.; Perry, J. Fluororenyl-ethynperylene derivatives with strong two photon absorption: Influence of substituents on optical properties. *J. Mater. Chem.* **2015**, *C3*, 3730–3744.
70. Liu, X.T.; Reu, A.M.; Guo, J.F.; Sun, Y.; Huang, S.; Feu, J.K. Theoretical investigation of one- and two-photon spectra of pyrazabole chromophores. *Theor. Chem. Acc.* **2011**, *130*, 37–50. [[CrossRef](#)]
71. Liu, Y.; Nolte, D.D.; Pyrak-Nolte, L. Large format fabrication by two-photon polymerization. *Appl. Phys.* **2010**, *100A*, 181–191. [[CrossRef](#)]
72. Liu, Y.; Hu, Q.; Zhang, F.; Tuck, C.; Irvine, D.; Hague, R.; He, Y.; Simonelli, M.; Rance, G.A.; Smith, E.F.; et al. Additive Manufacture of Three Dimensional Nanocomposite Based Objects through Multiphoton Fabrication. *Polymers* **2016**, *8*, 325. [[CrossRef](#)] [[PubMed](#)]
73. Moura, G.L.; Simas, A.M. Two photon absorption of fluorine derivatives: Systematic molecular design. *J. Phys. Chem.* **2010**, *114*, 6106–6116.
74. Terenziani, F.; Katan, C.; Badaeva, E.; Tretiak, S.; Blanchard-Desce, M. Enhanced two-photon absorption of organic chromophores: Theoretical and experimental assessments. *Adv. Mater.* **2008**, *20*, 4641–4687. [[CrossRef](#)]
75. Cumpston, B.H.; Ananthavel, S.P.; Barlow, S.; Dyer, D.L.; Ehrlich, J.E.; Erskine, L.L.; Heikal, A.A.; Kuebler, S.M.; Lee, I.-Y.S.; McCord-Maughon, D.; et al. Two-photon polymerization initiators for three-dimensional optical data storage and microfabrication. *Nature* **1999**, *398*, 51–54. [[CrossRef](#)]
76. Lee, K.S.; Kim, S.O.; Yang, H.K.; Sao, B.K.; Sun, H.B.; Kowata, S.; Fleitz, P. Lithographic microfabrication by using two photon absorbing phenylene-vinylene derivatives. *Molecular Crystals. Liq. Cryst.* **2004**, *424*, 35–41. [[CrossRef](#)]
77. Lee, K.S.; Kim, R.H.; Yang, D.Y.; Park, S.H. Advances in 3D Nano/microfabrication using two photons induced polymerization. *Prog. Polym. Sci.* **2008**, *33*, 631–681. [[CrossRef](#)]
78. Chakrabarti, S.; Ruud, K. Large two photon absorption cross section: Molecular tweezer as a new promising class of compounds for nonlinear optics. *Physical Chemistry. Chem. Phys.* **2009**, *11*, 2592–2596. [[CrossRef](#)]
79. Park, S.H.; Lee, S.H.; Yang, D.Y. Sub-regional slicing method to increase three-dimensional nanofabrication efficiency in two-photon polymerization. *Appl. Phys. Lett.* **2005**, *87*, 154108. [[CrossRef](#)]
80. Park, S.H.; Yang, D.Y.; Lee, K.S. Two-photon stereo-lithography for realizing ultraprecise three-dimensional Nano/micro-devices. *Laser Photonics Rev.* **2009**, *3*, 1–11. [[CrossRef](#)]
81. Skoog, S.A.; Goering, P.L.; Narayan, R.J. Stereolithography in tissue engineering. *J. Mater. Sci. Mater. Med.* **2010**, *25*, 845–856. [[CrossRef](#)]
82. Ovsianikov, A.; Farsari, M.; Chichkov, B. Photonic and biomedical applications of the two photon polymerization technique. In *Stereo-Lithography. Materials. Processes and Applications*; Bartolo, P.J., Ed.; Springer: New York, NY, USA, 2011.

83. Farsari, M.; Chichkov, B.N. Two-photon fabrication. *Nat. Photon.* **2009**, *3*, 450–452. [[CrossRef](#)]
84. Zhao, Y.; Li, X.; Wu, F.; Fang, X. Novel multi-branched two-photon-polymerization initiators of keto-coumarin derivatives. *J. Photochem. Photobiol.* **2006**, *177A*, 12–16. [[CrossRef](#)]
85. Geng, Q.; Wang, D.; Chen, P.; Chen, S.C. Ultrafast multi-focus 3-D nano-fabrication based on two-photon polymerization. *Nat. Commun.* **2019**, *10*, 2179. [[CrossRef](#)] [[PubMed](#)]
86. Berg, A.; Wyrwa, R.; Weisser, J.; Weiss, T.; Schade, R.; Hildebrand, G.; Liefelth, K.; Schneider, B.; Ellinger, R.; Schnabelrauch, M. Synthesis of Photopolymerizable Hydrophilic Macromers and Evaluation of Their Applicability as Reactive Resin Components for the Fabrication of Three-Dimensionally Structured Hydrogel Matrices by 2-Photon-Polymerization. *Adv. Eng. Mater.* **2011**, *13*, B274–B284. [[CrossRef](#)]
87. André, J.C.; Gallais, L. Procédé pour la Réalisation d'un Objet Tridimensionnel par un Processus de Photo-Polymérisation Multi-Photonique et Dispositif Associé Utilisant des Nanoparticules. French Patent FR 1852698, 28 March 2018.
88. André, J.C.; Gallais, L.; Amra, C. Procédé Pour la Réalisation d'un Objet Tridimensionnel par un Processus de Photopolymérisation Multi-Photonique et Dispositif Associé. French Patent 16-59211, 28 September 2016.
89. André, J.C.; Gallais, L.; Amra, C.; Zerrad, M. Procédé de Fabrication d'un Objet Tridimensionnel. ou de Modification de l'état de Surface d'un Objet Préformé. par Photopolymérisation. French Patent FR 1908646, 4 February 2021.
90. Surkamp, N.; Zyla, G.; Gurevich, E.L.; Klehr, A.; Knigge, A.; Ostendorf, A.; Hofmann, M.R. Mode-locked diode laser-based two-photon polymerization. *Electron. Lett.* **2020**, *56*, 91–93. [[CrossRef](#)]
91. Doualle, T.; André, J.C.; Gallais, L. 3D-printing of silica glass through multiphoton polymerization process. *Opt. Lett.* **2021**, *46*, 364–367. [[CrossRef](#)]
92. Carlotti, M.; Mattoli, V. Functional Materials for Two-Photon Polymerization in Microfabrication. *Small* **2019**, *15*, e1902687. [[CrossRef](#)]
93. Bagheri, A.; Jin, J. Photo-polymerization in 3D Printing. *ACS Appl. Polym. Mater.* **2019**, *1*, 593–611. [[CrossRef](#)]
94. Sängler, J.; Pauw, B.R.; Sturm, H.; Günster, J. First time additively manufactured advanced ceramics by using two-photon polymerization for powder processing. *Open Ceram.* **2020**, *4*, 100040. [[CrossRef](#)]
95. Kotz, F.; Quic, A.S.; Risch, P.; Martin, T.; Hoose, T.; Thiel, M.; Helmer, D.; Rapp, B.E. Two-Photon Polymerization of Nanocomposites for the Fabrication of Transparent Fused Silica Glass Microstructures. *Adv. Mater.* **2021**, *33*, 2006341. [[CrossRef](#)]
96. Regehly, M.; Garmshausen, Y.; Reuter, M.; König, N.F.; Israel, E.; Kelly, D.P.; Chou, C.Y.; Koch, K.; Asfari, B.; Hecht, S. Xolography for linear volumetric 3D printing. *Nature* **2020**, *588*, 620–624. [[CrossRef](#)] [[PubMed](#)]
97. André, J.C. Impression 3D «volumique»: Du décimètre au mm? *Tech. L'ingénieur* **2022**, RE289. Available online: <https://www.techniques-ingenieur.fr/base-documentaire/mecanique-th7/enjeux-procedes-et-marches-42686210/impresion-3d-volumique-du-decimetre-au-m-re289/vers-le-principe-de-l-impresion-3d-volumique-re289niv10001.html> (accessed on 27 May 2023).

Disclaimer/Publisher's Note: The statements, opinions and data contained in all publications are solely those of the individual author(s) and contributor(s) and not of MDPI and/or the editor(s). MDPI and/or the editor(s) disclaim responsibility for any injury to people or property resulting from any ideas, methods, instructions or products referred to in the content.